Experimental Validation of Image-Based Modeling of Torso Surface Potentials During Acute Myocardial Ischemia

Brian Zenger[1,2,3,4], Jake A Bergquist[1,2,4], Wilson W Good[1,2,4], Brett M Burton[1,2,4], Jess D Tate[1], Rob S MacLeod[1,2,3,4]

[1] Scientific Computing and Imaging Institute, SLC, USA
[2] Nora Eccles Cardiovascular Research and Training Institute, SLC, USA
[3] School of Medicine, University of Utah, SLC, USA
[4] Department of Biomedical Engineering, University of Utah, SLC, USA

Abstract

Myocardial ischemia is an early clinical indicator of several underlying cardiac pathologies. Significant progress has been made in computing body-surface potentials from cardiac sources by solving the forward problem of electrocardiography. However, the lack of in vivo studies to validate such computations from ischemic sources has limited the translational potential of such models. We have developed a large-animal experimental model that includes simultaneous recordings within the myocardium, on the epicardial surface, and on the torso surface during episodes of acute, controlled ischemia with comprehensive imaging and subject specific modeling for each animal. We then identified ischemic sources and used the finite element method to solve a static bidomain equation on a geometric model to compute torso surface potentials. Across 33 individual heartbeats, the forward computed torso potentials showed only moderate agreement in both pattern and amplitude with Pearson's correlation coefficient, root mean squared error, and absolute error varying significantly by heartbeat (-0.05 ± 0.19, 0.10 ± 0.03*mV, and* 0.11 ± 0.03 *mV, respectively). Qualitative analysis showed a more encouraging pattern of elevations and depressions shared by computed and measured torso potentials. Further studies will focus on characterizing these sources of error and understanding how they effect the study results.*

1. Introduction

Acute myocardial ischemia is a transient and dynamic clinical indicator of multiple cardiovascular diseases, including coronary artery disease, Takatsobu cardiomyopathy, and coronary artery dissection [1–3]. Myocardial ischemia occurs when there is inadequate perfusion to regions of the heart tissue, leading to local oxygen deprivation and accumulation of toxic metabolites [4, 5]. Within seconds to minutes, the results include changes in ion concentrations and cellular pH, which in turn alter the normal electrical signature of the heart, visible on the body surface through the electrocardiogram. However, electrocardiographic detection methods of myocardial ischemia are poor, with sensitivities ranging from 55–65% [6, 7].

This project had twofold motivation. The first was the lack of experiments able to capture potentials within the heart and on the heart and torso surfaces in large mammal models. Such information is necessary to explore relationships between underlying pathophysiology and clinical manifestations. The second motivation is to generate data to validate both simulations and reconstructions from ECG imaging (ECGI) of acute ischemia. Our group has used intramyocardial measurements during ischemia that have revealed a novel configuration of the sources of cardiac potentials during especially nontransmural ischemia.[8] However, we have not previously acquired body surface potentials under these conditions, the critical link required to translate our results to clinical practice. We have also carried out simulations of epicardial and body surface potentials from experimentally derived ischemic zones. While we have compared these computed epicardial potentials to measured values obtained during experiments [9, 10], we had previously been unable to obtain the associated body-surface potentials necessary to complete this investigation and explore its translational impact. To address the translational shortcomings of previous preparations, we modified our experimental model to simultaneously record electrograms within the myocardium, and on the heart surface, and ECG's on the torso surface of an animal with re-closed chest during controlled episodes of acute myocardial ischemia [11]. We then incorporated a homogeneous, isotropic, experiment-specific torso volume to our forward solution and compared the results to the experimentally recorded potentials.

 ISSN: 2325-887X DOI: 10.22489/CinC.2019.417

2. Methods

2.1. Animal Experiments

We performed six animal experiments using the approaches described in [12]. Briefly, intramural cardiac signals were sampled with needle electrodes comprised of 10 contacts spaced every 1.8 mm along the shaft of the needle. Each study included 15–25 intramural needle electrodes placed in the region of the myocardium affected by acute myocardial ischemia. The heart surface was sampled by a 247-lead epicardial sock array that evenly distributed electrodes within 7–8 mm on the surface of the ventricles. The torso surface was measured with 72–96 surface electrodes, depending on the torso surface available. The electrodes were strips of 12 Ag/AgCl contacts evenly spaced 3 cm apart. All electrical signals were recorded using a custom multiplexer and sampled at 1 kHz [10, 12].

Ischemic episodes were induced by varying the coronary blood supply and metabolic demand of the heart. The supply was modulated using a calibrated hydraulic occluder placed around the left anterior descending coronary artery (LAD). The demand of the heart was modulated via either right atrial pacing or continuous dobutamine infusion. Ischemic episodes lasted 15 minutes, during which demand was increased every 3 minutes. Following each ischemic episode, the heart was given time to recover.

Recorded signals were processed using our PFEIFER signal processing toolkit [13]. The signals were filtered, baseline corrected, and annotated then regions of ischemia within the myocardium were identified by elevated local ST40 potentials *i.e.,* measured at 40% of the ST segment, above 4.5 mV.

2.2. Image-Based Geometric Model

To create subject-specific models of anatomy and electrode position, we acquired body magnetic resonance images (MRIs) immediately postmortem using a 3T Prisma scanner (Siemens Medical). The heart was then excised, and high-resolution MRIs were obtained using a 7T Bruker (BIOSPEC 70/30, Billerica, MA), with fast imaging with steady-state precession (FISP), fast low-angle shot (FLASH), and diffusion tensor (DTI) imaging sequences. The DTI images identified principle myocardial fiber orientation vectors that were used in the forward model solution to define anisotropic longitudinal and transverse conductivity values (shown in table **??**). The high-resolution images were registered to the whole body images using an affine registration. The sock electrode array position was registered to the heart surface using our GRÖMeR pipeline [14]. The heart, blood, lungs, bones, and other major anatomical structures were delineated using the Seg3D segmentation software (SCI, University of Utah, SLC, USA). A whole body computational model was then meshed using the Cleaver meshing software (SCI, University of Utah, SLC, UT).

2.3. Forward Model Solution

The forward model solution was formulated similarly to our previous studies [9, 10]. To summarize this formulation, the passive biodomain model was used to calculate the torso surface extracellular potentials shown in equation 1

$$\nabla \cdot (\bar{\sigma}_e + \bar{\sigma}_i)\nabla\phi_e = -\nabla \cdot \bar{\sigma}_i \nabla V_m, \tag{1}$$

where $\bar{\sigma}_e$ and $\bar{\sigma}_i$ represent the extracellular and intracellular anisotropic conductivity values, respectively, and V_m and ϕ_e represent transmembrane and extracellular potentials throughout the heart. Experimentally derived ischemic zones and healthy zones were assigned transmembrane potential values of 35 mV and 0 mV, respectively, based on experimental patch clamp recordings performed previously [15]. The border zone between normal and healthy tissue transitioned using a two phase exponential decay function described in [16],

$$V_{BZ}(d) = \begin{cases} V_m e^{\frac{-d^2}{2\sigma^2}} & d < S_1 \\ V_m e^{\frac{-(S_1)^2}{\sigma^2}}(1 - \frac{d-S_1}{S_2-S_1}) & S_1 \leq d < S_2 \\ 0 & d \geq S_2 \end{cases} \tag{2}$$

where V_m is the transmembrane potential, S_1 is the distance at which the border zone function transitions from Gaussian to linear, and S_2 defines the distance at which the border zone ends. Anisotropic myocardial, and isotropic blood, and torso conductivities were assigned as described previously.[17] A no-flow Neumann boundary condition was applied at the torso surface, and Cauchy boundary conditions were applied at the endocardium and epicardium.

The system of equations was then solved using the linear finite element model with an iterative solver to compute ϕ_e using a conjugate gradient method with a Jacobi preconditioner within the SCIRun problem-solving environment (SCI, University of Utah, SLC, USA). Data were visualized using SCIRun and *map3d* visualization tools (SCI, University of Utah, SLC, USA).

2.4. Data Analysis

The forward computed torso potentials were compared with measured torso-surface potentials using both visualization and statistical metrics. Pearson's correlation coefficient (PCC), RMS error (RMSE), and absolute error (AE)

Table 1. Statistics calculated for the 33 beats reported from the study.

PCC	RMSE	AE
-0.05 ± 0.19	0.10 ± 0.03mV	0.11 ± 0.03 mV

were used to quantify agreement.

$$\begin{aligned} \text{PCC} &= \frac{\mathbb{E}((\phi - \mu_\phi)(\phi_\gtrdot - \mu_{\phi_\gtrdot}))}{SD_{\phi_c} SD_{\phi_m}} \\ \text{RMSE} &= \sqrt{\mathbb{E}((\phi - \phi_\gtrdot)^{\not\leq})} \\ \text{AE} &= |\phi_c - \phi_m|, \end{aligned} \tag{3}$$

where ϕ_c and ϕ_m are the simulated and measured potentials, respectively, and SD_{ϕ_c} and SD_{ϕ_m} are the standard deviations of simulated and measured potentials, respectively.

3. Results

A statistical summary from 33 individual beats with forward-computed and experimentally recorded torso-surface ST40 potentials are shown in table 1. Qualitative analysis showed similar patterns between the measured and computed torso potentials. In general, there was one distinct site of depression and elevation in both torso maps. The elevation was located on the left-lateral chest wall and the depression was over the right and superior torso surfaces. Figure 1 shows an example of the measured and computed torso potentials.

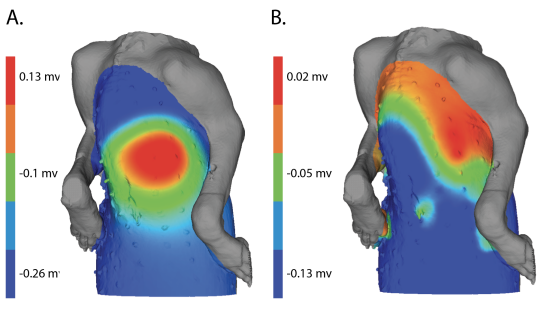

Figure 1. Image of computed and measured potentials on the torso surface A. Forward-computed ST40 potential values. B. Experimentally measured ST40 potential values.

4. Discussion

In this study, we compared, for the first time, forward-computed and experimentally measured torso-surface potentials from bioelectric ischemic sources during an episode of controlled ischemia. Our qualitative results showed similar patterns but statistical analysis showed significant variability in the forward-computed and experimentally measured values.

Overall, the PCC was lower and the RMSE and AE values were larger than expected and indicate the need for improvement. We speculate several key sources of error in our computation including signal to noise ratio in the torso surface recordings, registration of electrode and anatomical locations, assumptions about torso conductivities, and assigning the "transition zone" between ischemic and non-ischemic tissues. First, there was significant noise within our recorded torso surface signals. When measuring very small (100–200 μV amplitudes of ST segment deflection), small amounts of noise can significantly perturb the calculated ST40 value. Next, our registration of heart position and electrode locations introduced possibilities for significant error. The MRI imaging on which the model construction is based, occurred shortly after the experiment with a static torso and deflated lungs. The resulting torso maps showed a spatial shift between measured and computed potentials that could originate from a poor initial registration. To mitigate these errors we will use optimization approaches to quantify where sources of registration error exist and determine if these errors are significantly perturbing the computed potentials. Next, previous studies have incorporated other tissue conductivities within the torso, *e.g.,* lungs. We suspect that regional changes in conductivities could have contributed to shape variations of depressions and elevations on the torso. Finally, our current model of the transition zone between normal and ischemic tissues assumes a uniform voltage step over the entire boundary between the ischemic and healthy tissue. However, our extracellular recordings show substantial variation over this zone, suggesting that a uniform transition zone does not adequately characterize the complex nature of ischemic sources. We speculate that incorporating a variable transition between ischemic and healthy tissue based on extracellular recordings will improve the accuracy of the computed potentials.

Future work will incorporate non-uniform border zone based on experimental recordings by creating a mapping between measured extracellular potentials and assigned transmembrane potentials. We will also incorporate torso conductivity inhomogeneities by adding lungs identified from our whole-body imaging. Finally, we will also increase the number of experiments for more in-depth analysis. Achieving acceptable fidelity of the forward solution using this preparation will then allow exploration of the

associated ECG imaging reconstructions and advance the field.

Acknowledgments

Support for this research came from the NIH NIGMS Center for Integrative Biomedical Computing (www.sci.utah.edu/cibc), NIH NIGMS grant no. P41GM103545 and the Nora Eccles Treadwell Foundation for Cardiovascular Research.

References

[1] Safdar B, Ong P, Camici PG. Identifying Myocardial Ischemia due to Coronary Microvascular Dysfunction in the Emergency Department: Introducing a New Paradigm in Acute Chest Pain Evaluation. Clinical Therapeutics 2018; 1–11. ISSN 01492918.

[2] Jespersen L, Abildstrøm SZ, Hvelplund A, Prescott E. Persistent angina: highly prevalent and associated with long-term anxiety, depression, low physical functioning, and quality of life in stable angina pectoris. Clinical Research in Cardiology 2013;102(8):571–581. ISSN 1861-0692.

[3] Noel BMC, J. PC, Norine WM, L. FJ, G. CP, M. CW, Austin CJ, S. CL, Filippo C, Marcelo DC, S. DP, S. GZ, Paul G, M. HE, Ahmed H, A. HJ, S. HJ, Erin I, Ruth K, N. LG, Peter L, Joao L, Puja M, Patrice DN, Michelle O, D. PG, A. QA, Harmony R, British R, George S, Viviany T, Janet W, Nanette W. Ischemia and No Obstructive Coronary Artery Disease (INOCA). Circulation March 2017;135(11):1075–1092.

[4] Hearse D. Myocardial ischaemia: Can we agree on a definition for the 21^{st} century? Cardiovasc Res 1994;28:1737–1744.

[5] Falk E, Shah P, de Feyter P. Ischemic Heart Disease. 1 edition. London, England: Manson Publishing, 2007.

[6] Knuuti J, Ballo H, Juarez-Orozco LE, Saraste A, Kolh P, Rutjes AWS, Jüni P, Windecker S, Bax JJ, Wijns W. The performance of non-invasive tests to rule-in and rule-out significant coronary artery stenosis in patients with stable angina: A meta-analysis focused on post-test disease probability. European Heart Journal 2018;39(35):3322–3330. ISSN 15229645.

[7] Stern S. State of the art in stress testing and ischaemia monitoring. Card Electrophysiol Rev September 2002;6(3):204–208.

[8] Aras K, Burton B, Swenson D, MacLeod R. Spatial organization of acute myocardial ischemia. J Electrocardiol 2016; 49(3):689–692.

[9] Burton B, Aras K, Good W, Tate J, Zenger B, MacLeod. R. Image-based modeling of acute myocardial ischemia using experimentally derived ischemic zone source representations. J Electrocardiol 2018;51(4):725–733.

[10] Burton B, Aras K, Good W, Tate J, Zenger B, MacLeod. R. A framework for image-based modeling of acute myocardial ischemia using intramurally recorded extracellular potential. Annal Biomed Eng 2018;46(9):1325–1336.

[11] Zenger B, Good WW, Bergquist JA, Tate JD, Sharma V, Macleod RS. Electrocardiographic Comparison of Dobutamine and BRUCE Cardiac Stress Testing With High Resolution Mapping in Experimental Models. Computing in Cardiology 2018;45:1–4.

[12] Zenger B, Good WW, Bergquist JA, Tate JD, MacLeod RS. In situ methods paper. Technical Report 0, Inst, 2019. In Preparation.

[13] Rodenhauser A, Good W, Zenger B, Tate J, Aras K, Burton B, MacLeod R. Pfeifer: Preprocessing framework for electrograms intermittently fiducialized from experimental recordings. J Open Source Software 2018;3(21):472.

[14] Bergquist JA, Good WW, Zenger B, Tate JD, MacLeod RS. Grömer: A pipeline for geodesic refinement of mesh registration. Technical Report 1, Inst, Accepted 2019. Accepted.

[15] Li D, Li C, Yong A, Kilpatrick D. Source of electrocardiographic ST changes in subendocardial ischemia. Circ Res 1998;82:957–970.

[16] Swenson D, Stinstra J, Burton B, Aras K, Healy L, , MacLeod R. Evaluating the effects of border zone approximations with subject specific ischemia models. In Doessel O, Schlegel WC (eds.), World Congress on Med. Phys. and Biomed. Eng., volume 25/IV. Heidelberg: Springer, 2009; 1680–1683.

[17] Stinstra J, Weinstein D, Hopenfeld B, Henriquez C, MacLeod R. Software challenges in the new field of integrated cardiac models. j IJBEM 2005;7(1):195–198.

Address for correspondence:

Brian Zenger
72 Central Campus Dr, Salt Lake City, UT 84112
zenger@sci.utah.edu